THE ASTROPHYSICAL JOURNAL, 599:L13–L16, 2003 December 10

HOT DUST IN RADIO-LOUD ACTIVE GALACTIC NUCLEI

WOLFRAM FREUDLING
Space Telescope–European Coordinating Facility, European Southern Observatory, Karl-Schwarzschild-Strasse 2, D-85748 Garching, Germany; wfreudli@eso.org
RALF SIEBENMORGEN
European Southern Observatory, Karl-Schwarzschild-Strasse 2, D-85748 Garching, Germany; rsiebenm@eso.org
AND
MARTIN HAAS
Astronomisches Institut der Ruhr-Universität Bochum, Universität Strasse 150, D-44780 Bochum, Germany; haas@astro.ruhr-uni-bochum.de
Received 2003 September 4; accepted 2003 October 30; published 2003 November 17

ABSTRACT

We have measured mid-infrared (MIR) fluxes of 3C sources on images taken with ISOCAM on board the *Infrared Space Observatory* (*ISO*). The photometric data were combined with existing photometry at other wavelengths to assemble the spectral energy distribution (SED) for each galaxy from infrared to radio wavelengths. In addition, we used ISOPHOT spectra to compute average MIR spectra for different types of active galactic nuclei (AGNs). The MIR emission of 53 of our sources shows evidence of dust. We find a clear correlation between the SEDs, emission from polycyclic aromatic hydrocarbons (PAHs), and the type of AGN. Specifically, we find that in broad emission line radio galaxies (BLRGs), the dust emission peaks at $\lambda \approx 40$ μm and PAH bands are weak, whereas emission in comparable narrow-line radio galaxies (NLRGs) peaks at a longer wavelength of $\lambda \approx 100$ μm and the PAH bands are much stronger. Although less pronounced, a similar trend is seen when comparing QSOs with high-luminosity NLRGs. We used dust radiative transfer models with a central heating source to describe the SEDs. The difference in the dust emission appears to be the effect of heating by radiation from the central engine. In type 1 AGNs (BLRGs and QSOs), the broad-line region (BLR) is directly visible, and therefore hot ($T \gtrsim 300$ K) dust dominates the emission. In this region, PAHs are destroyed, which explains the weak PAH emission. On the other hand, the BLR is hidden in type 2 AGNs (NLRGs). Their SEDs are therefore dominated by cooler dust, including PAHs.

Subject headings: dust, extinction — galaxies: active — galaxies: ISM — infrared: galaxies — quasars: general

1. INTRODUCTION

The widely accepted paradigm for the power source of active galactic nuclei (AGNs) is a massive black hole. In this picture, accretion of dust and gas powers the AGN. Beamed radiation escapes from the central engine and affects the surrounding gas and dust. The effect on gas can directly be observed in close-by AGNs through the spatial separation of ionized and neutral gas (e.g., Tadhunter & Tsvetanov 1989; Prieto & Freudling 1993). The impact of this radiation on dust, if present, is expected to be similarly dramatic. The intense radiation field in the immediate vicinity of the central engine prevents dust from forming and evaporates any dust approaching that region. In this region, polycyclic aromatic hydrocarbons (PAHs) cannot exist. At somewhat larger distances from the nucleus, the radiation field heats the dust to just below its evaporation temperature. Dust at such distances will have temperatures of about 1500 K. Cold dust ($T \lesssim 50$ K) should exist only at distances greater than several hundred parsecs to a few kiloparsecs. At intermediate distances, a region should exist where large quantities of dust are significantly heated by the AGN to temperatures of a few hundred kelvins and should therefore be detectable at mid-infrared (MIR) wavelengths.

Unfortunately, detailed mapping of dust temperatures in AGN host galaxies is not feasible at present. Our knowledge of dust in 3C sources is therefore based on low spatial resolution photometry. Observations with the *Infrared Astronomical Satellite* (*IRAS*) showed that 3C sources, which are bright at $\lambda = 60$ μm, are typically much fainter or not detectable at $\lambda = 12$ μm (Heckman et al. 1994 and references therein). This signature of cold dust is also seen in the more recent data presented by Meisenheimer et al. (2001). Heckman et al. (1994) find that the narrow-line radio galaxies (NLRGs) are about a factor of 4–5 fainter in the MIR than broad emission line radio galaxies (BLRGs) but are similar to BLRGs at $\lambda = 60$ μm. These differences are qualitatively consistent with unification schemes, since hotter dust is visible in BLRGs because of their viewing angle.

ISOCAM was more than an order of magnitude more sensitive than *IRAS* at MIR wavelengths. It was able to detect the hot dust component in 3C sources at much higher redshifts and therefore expand comparison of type 1 and 2 AGNs to a much wider range of luminosities. In this letter, we report first results from a program to investigate the hot dust component in 3C sources based on ISOCAM observations. A detailed discussion of our data reduction and modeling procedures, as well as a full presentation of our data, are deferred to a later paper (R. Siebenmorgen et al. 2003, in preparation, hereafter SFKH).

2. OBSERVATIONS AND DATA REDUCTION

2.1. *The Sample*

The goal of our program is to investigate dust emission in AGNs and, in particular, to search for differences related to the orientation of the central engine. Constraining the spectral energy distribution (SED) emission of both hot and cold dust requires infrared photometry covering the full wavelength range from micron to millimeter wavelengths. We used the 3CR catalog as our parent catalog because its 178 MHz selection should be essentially unbiased in its inclusion of AGNs at different viewing angles. In addition, photometric measurements at far-infrared and millimeter wavelengths are available for large subsamples of the catalog (e.g., Meisenheimer et al. 2001; M. Haas et al. 2003, in preparation). By complementing these available data with our new MIR mea-

surements, we were able to construct SEDs from optical to millimeter wavelengths.

We have compiled our sample by cross-correlating the position of 3C sources with the list of ISOCAM observations available from the *Infrared Space Observatory* (*ISO*) post mission archive. We then extracted all ISOCAM images that potentially include 3C sources. Each reduced image was visually inspected, and the pointing of the spacecraft was verified using stellar and other sources contained in the images. We report here on that subsample of our data for which the combined ISOCAM photometry, data from the literature, and ISOPHOT photometry by M. Haas et al. (2003, in preparation) suffice to constrain the full infrared SED of our sources.

2.2. *Data Reduction*

ISOCAM images in the *ISO* archive have been obtained for a variety of programs and purposes and therefore vary in depth, resolution, used wavelength band, and dither strategy. We reprocessed the raw data using a common set of procedures aimed at obtaining the best possible calibration and homogeneity of our photometric measurements. We followed the ISOCAM handbook (Blommaert et al. 2001)[1] and used the CIA software (Ott, Pollock, & Siebenmorgen 2000) to subtract darks, remove cosmic-rays hits, remove the effect of flux transients, and finally flat-field, resample, and co-add the individual exposures. The typical useful field of view of the images is about 1.5×1.5 arcmin^2 sampled with 3×3 arcsec^2 pixels. Most of the detected 3C sources were not or only barely spatially resolved by ISOCAM. In those cases, apertures with a radius of 10″ were used, and aperture losses were modeled using synthetic point-spread functions.[2] For extended sources, we chose apertures that measure the spatially integrated flux of the source.

For most 3C sources, photometric information at optical, near-infrared and/or far-infrared, and millimeter wavelengths is available. We compiled SEDs between 0.5 and 1300 μm for all sources in our sample using data listed in the NASA Extragalactic Database, the ISOPHOT measurement given in M. Haas et al. (2003, in preparation), and other recent papers (see SFKH). In compiling the SEDs, we used only photometric data, which include, like our own ISOCAM photometry, the integrated flux from the whole host galaxy. For each SED, we estimated the contribution of synchrotron radiation to the MIR fluxes by extrapolating the radio core flux. We found that the synchrotron radiation is a negligible contribution to the MIR flux for all SEDs used in this paper.

3. RESULTS

We retrieved ISOCAM images for a total of 88 sources. The rms noise in the reduced images ranges from 0.5 to 5 mJy. We detected a total of 71 galaxies. The high detection rate indicates that hot dust is common in radio-loud AGNs, and that 3C sources are bright enough in the MIR so that they will be readily accessible to detailed studies by future instruments such as *SIRTF*.

A steep rise of the flux from optical wavelengths below 1 μm to the MIR indicates the presence of a significant amount of dust at $T \approx 300$ K for a large fraction of our sample. In order to estimate the contribution of stars to the MIR, we fitted 4000 K blackbody spectra to the short wavelength part of the SEDs. This temperature deliberately was taken to be on the low side of the range of possible average stellar temperatures so that the MIR emission attributed to stars is an upper limit. Taking this stellar contribution into account, we found clear evidence of dust in 53 sources, i.e., 60% of our initial sample. The highest redshift source with a clear detection of hot dust is 3C 324 at a redshift of 1.2. For a total of 27 sources, our data suffice to construct SEDs. The measured *ISO* fluxes for them are presented in Table 1.

4. SED MODELING

Interpretation of the IR spectra requires detailed knowledge of the energy sources and the distribution and composition of gas and dust that absorbs and retransmits the radiation. In the case of the AGNs discussed in this paper, the primary energy source is the central engine in the nucleus enshrouded by dust clouds. Dust close to the nucleus absorbs the radiation from the nucleus and reradiates it. This emission depends mostly on the total power and spectrum of the central engine and the distribution and properties of dust. While the composition of the dust can be reasonably assumed to be similar to local dust and is therefore well constrained, its distribution around the power source of the AGN is largely unknown. It is generally assumed that the geometrical distribution of dust around AGNs is similar to a torus or warped disk (e.g., Urry & Padovani 1995). However, observations of dust features close to the nucleus of AGNs with *HST* reveal a variety of morphologies (Martel et al. 2000). These observations and the fact that dust at distance much larger than the size of the putative torus shapes the MIR spectrum (Farrah et al. 2003) motivated us to adopt a simple approach to the modeling of dust SEDs in AGNs. Instead of choosing between possible geometrical configurations, we carried out spherical radiative transfer calculations with a central heating source. In this approach, the size of the model sphere depends on the viewing angle because of the intrinsic asymmetry of AGNs. We used a power law $L \propto \nu^{-0.7}$ between $\lambda = 10$ Å and 2 μm as the input spectrum of the central sources. The exciting radiation field is therefore significantly harder than for starbursts leading to stronger photodestruction of small grains (Siebenmorgen, Krügel, & Spoon 2003). Had we used a more distributed source of energy within the nucleus, the predicted PAH emission would have been much stronger. We numerically solved the radiative transfer equations for a grid of models, varying the total luminosity of the central engine, the total extinction, and the outer radius of the dust clouds. The dust in our model consists of carbon grains, silicate grains, and PAHs. The initial density within the sphere is constant, but dust evaporation and PAH destruction are taken into account in a self-consistent way. We computed model SEDs for outer radii ranging from 0.125 to 16 kpc, luminosities ranging from 10^9 to 10^{14} $L_\odot$, and visual extinction ranging from 1 to 128 mag.[3] The parameters of the best-fitting model for each observed SED are listed in Table 1. In our modeling, all emission from the central engine is reprocessed by dust. The input power to our models is therefore identical to the total dust luminosity, which we use below to divide our sample into subsamples.

5. DISCUSSION

5.1. *Averaged SEDs*

In order to investigate differences in dust emission for type 1 and 2 AGNs, we divided our sample into four different subsamples. Type 1 AGNs were subdivided into BLRGs and QSOs. Type 2 AGNs with dust luminosities fainter then 10^{11} $L_\odot$ were assigned to a low-luminosity NRLG subsample and those as bright or brighter than this limit to an equivalent high-luminosity subsample. This luminosity limit was chosen so that the average dust lumi-

[1] See http://www.iso.vilspa.esa.es.

[2] K. Okumura 1998, ISOCAM PSF Report, available at http://www.iso.vilspa.esa.es/users/expl_lib/CAM_list.html.

[3] The full set of models is available at http://www.eso.org/~rsiebenm/agn_models.

TABLE 1
ISOCAM Observations of 3C Sources

Name	Type	$F_{\rm ISOCAM}$ (mJy)	Filter[a]	R (kpc)	log L^{b} ($L_{\odot}$)	A_V Magnitude
3C 006.1	NLRG	0.9 ± 0.2	10	16	11.75	32
3C 020	NLRG	5.3 ± 0.4	10	2	11.25	16
3C 031	LERG	25 ± 1	10	0.125	10.00	2
3C 033.1	BLRG	18 ± 1	10	0.125	11.25	16
3C 048	QSO	59 ± 4	3	4	12.75	32
3C 061.1	NLRG	0.9 ± 0.2	10	1	10.75	32
3C 071	NLRG	50830 ± 2540	3	2	11.50	16
3C 079	NLRG	21 ± 2	10	0.5	11.75	16
3C 084	NLRG	230 ± 20	2	2	11.25	4
3C 098	NLRG	24 ± 2	3	0.125	10.00	32
3C 249.1	QSO	19 ± 1	10	0.125	11.75	32
3C 277.3	BLRG	8.5 ± 0.5	3	0.25	10.50	1
3C 293	LERG	19 ± 2	10	8	10.75	2
3C 305	NLRG	21 ± 1	10	8	10.75	1
3C 309.1	QSO	8.2 ± 0.5	10	0.25	12.75	32
3C 321	NLRG	27 ± 1	10	2	11.50	16
3C 324	NLRG	1.7 ± 0.2	10	4	12.25	8
3C 330	NLRG	1.7 ± 0.2	10	0.125	11.75	32
3C 338	NLRG	8.8 ± 0.5	10	16	10.25	16
3C 351	QSO	32 ± 2	10	0.5	12.25	32
3C 356	NLRG	0.6 ± 0.2	10	4	12.25	64
3C 380	QSO	14 ± 1	10	1	12.50	32
3C 381	BLRG	19 ± 1	10	0.25	11.25	32
3C 382	BLRG	85 ± 5	10	0.125	11.00	2
3C 390.3	BLRG	94 ± 5	10	0.125	11.00	4
3C 445	BLRG	210 ± 11	3	0.125	11.50	16
3C 459	NLRG	29.5 ± 4	3	2	12.25	128

[a] ISOCAM Filters encoded as 2 = LW2 ($\lambda = 6.7$ μm), 10 = LW10 ($\lambda = 12.0$ μm), 3 = LW3 ($\lambda = 14.3$ μm).
[b] Based on $H_0 = 70$ km s^{-1} Mpc^{-1}, $\Omega_\Lambda = 0.70$, and $\Omega_m = 0.3$.

nosities of the high- and low-luminosity NLRGs resemble those of the QSOs and BLRGs, respectively. This subdivision also led to samples comparable in redshift and extended radio emission. Specifically, the mean redshift and extended radio luminosity of the high-luminosity NLRGs ($z = 0.53 \pm 0.4$ and $L_r = 10^{27.5\pm0.6}$ W Hz^{-1} sr^{-1}) match those of the QSOs ($z = 0.53 \pm 0.2$ and $L_r = 10^{27.1\pm1.1}$ W Hz^{-1} sr^{-1}), and the redshifts and radio luminosities of the low-luminosity NLRGs ($z = 0.06 \pm 0.06$ and $L_r = 10^{25.3\pm0.7}$ W Hz^{-1} sr^{-1}) resemble those of the BLRGs ($z = 0.11 \pm 0.06$ and $L_r = 10^{25.9\pm0.4}$ W Hz^{-1} sr^{-1}).

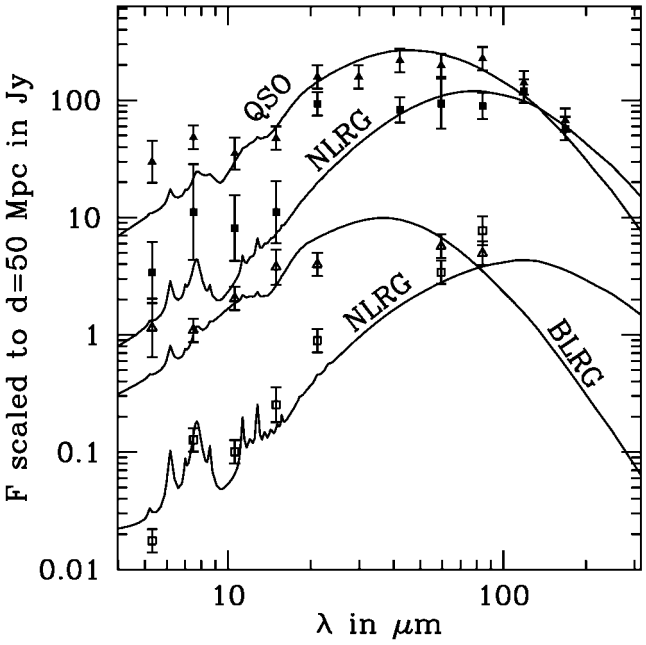

FIG. 1.—Mean SEDs for different AGN types. Filled triangle represent QSOs, filled squares represent NLRGs with $L_{\rm dust} > 10^{11}\ L_{\odot}$ (*black lines*), open triangles show BLRGs, and open squares show NLRGs with $L_{\rm dust} < 10^{11}\ L_{\odot}$. Error bars are the 1 σ uncertainty of the mean in each wavelength bin. The solid lines represent the corresponding averaged model for each AGN type.

We computed logarithmically averaged SEDs for each subsample to search for differences in their shapes. Specifically, the procedure we used was the following. First, we redshifted each observed SED to the rest frame and scaled it to the same interpolated flux at $\lambda = 25$ μm. Next, we computed logarithmic flux averages in wavelength bins. The averaged SEDs were then scaled so that their integrated fluxes equal the average of the integrated fluxes of all corresponding spectra. The same procedure without the wavelength binning was used on the model SEDs for each contributing source. The resulting averaged observed and model SEDs are shown in Figure 1. We have also used different averaging procedures and found that they did not alter the conclusions presented in this paper.

Figure 1 shows some clear and highly significant differences in the average SEDs of different AGN types. The dust emission peaks at $\lambda \approx 40$–50 μm for QSOs and BLRGs and around 70–100 μm for NLRGs. This difference in the peak wavelength by a factor of ~2 between type 1 and 2 objects seems to be virtually independent of luminosity. The difference reflects different temperature distributions of large dust grains and can be understood within the framework of unified models. For type 1 AGNs in which the broad-line region (BLR) is visible, unobscured hot dust dominates the SED. By contrast, the NLRG's large extinction obscures the BLR, and predominantly colder dust is visible.

5.2. *Strength of PAH Bands*

A more specific test of the heating mechanism is the strength of PAH bands. As discussed in § 4, the PAH strength is a sensitive indicator of the heating source because PAHs are destroyed by hard ionizing radiation. Despite the low spectral resolution of the

SEDs shown in Figure 1, some indications of the PAH bands are visible in the SEDs of the type 2 AGNs but not for the type 1 AGNs. This observation seems to confirm the destruction of PAHs near the central heating source.

We used ISOPHOT spectra of AGNs to investigate the strength of PAH bands as a function of AGN type in more detail. For that purpose, we assembled average spectra for each AGN type. Since radio-loud and radio-quiet AGNs have similar IR spectra (e.g., Sanders et al. 1989), we included both kinds of AGNs in those averages. We used the spectra presented by Haas et al. (2003) to compute an average QSO spectrum. For the BLRGs, we used ISOPHOT spectra of 3C sources available from the *ISO* archive and the Seyfert I spectra from Clavel et al. (2000). Finally, we used the average spectrum of Seyfert II galaxies presented by Clavel et al. (2000) as our average type 2 AGN spectrum. The flux of each averaged spectrum was scaled to the average of the corresponding AGN type in our 3C sample. These scaled spectra are presented in Figure 2.

The spectral index α was estimated by fitting $F_\lambda \propto \lambda^{-\alpha}$ to the continuum of the averaged spectra. We found $\alpha = -0.91 \pm 0.06$ for the QSOs, $\alpha = -0.70 \pm 0.03$ for the BLRGs, and $\alpha = -0.76 \pm 0.05$ for the Seyfert II galaxies. We note that because of the similarity between the 3C spectra of type 1 and Seyfert I spectra, the continuum slope as well as the PAH strength in our average spectrum of the BLRGs is indistinguishable from that of the average spectrum of Seyfert I galaxies shown in Figure 7 of Clavel et al. (2000).

A comparison of the three spectra in Figure 2 shows a clear difference between the PAH bands in spectra of AGNs of similar luminosity but different type. PAH bands in the spectra of type 2 AGNs are more than a factor of 3 stronger than in the corresponding type 1 spectra.

For comparison, we plotted the SED models shown in Figure 1 for the QSO, BLRG, and low-luminosity NRLG on top of the spectra in Figure 2. One can immediately recognize a basic correspondence between the continuum shapes and PAH strength of the models with the spectra. The fact that models fitted to the overall SEDs correctly predict the strength of the PAH bands in independent samples of the same AGNs type suggests a basic similarity in the physics within each of the different types of AGNs.

The relatively weak PAH bands in type 1 AGNs can be understood in terms of the unified models. In type 1 spectra, a large fraction of the visible flux originates from the BLR region where only few PAHs survive. This region is obscured in type 2 AGNs, and their spectra are hence dominated by cooler dust located at larger distances from the nucleus, where PAHs are shielded from the photodestruction. Type 1 and 2 AGN spectra differ because of the different relative contribution of hot dust to the total emission. When comparing spectra of AGNs with the same total *dust* luminosity, the different relative contribution of cold dust leads to the observed differences in the total PAH emission.

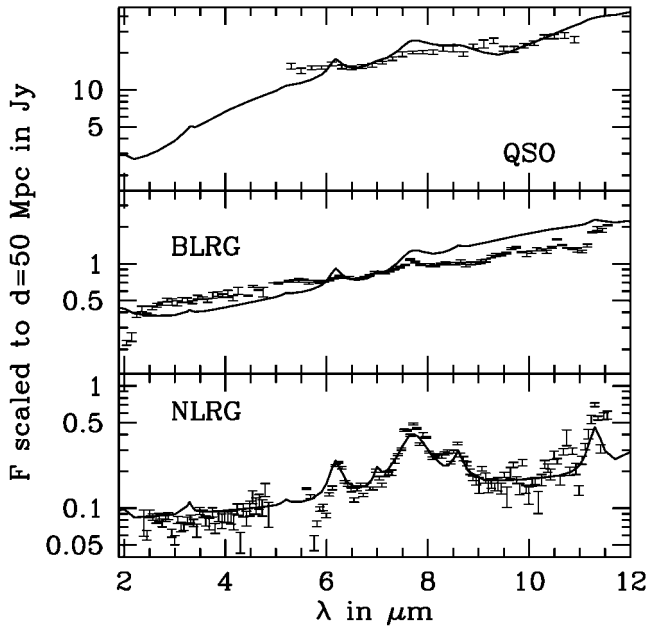

FIG. 2.—*Top*: Mean model spectrum of QSOs (*solid line*) in our sample superposed on the average ISOPHOT spectrum of PG quasars (*error bars*). *Middle*: mean model of BLRGs superposed on observed average ISOPHOT spectra (error bars). *Bottom*: Mean model SED of NLRGs with $L_{\rm dust} < 10^{11}\ L_\odot$ (*solid line*) superposed on observed average Seyfert 2 spectra (*error bars*).

6. SUMMARY AND CONCLUSION

We have detected hot dust in ISOCAM images of 3C galaxies out to redshift $z \approx 1.2$. We found a clear correlation between the type of the AGN and the overall SEDs in the sense that SEDs of BLRG and QSOs are dominated by emission from dust that is about a factor of 2 hotter than the one in comparable NRLGs. MIR spectra show that PAH emission bands in spectra of type 1 AGNs are significantly weaker than the ones in spectra of type 2 AGNs with the same total dust luminosity. These trends are naturally predicted if dust in AGNs is predominantly heated by hard radiation from a central engine that destroys PAHs close to the nucleus and heats larger dust grains at intermediate distances.

We thank Bernhard Schulz for providing digital versions of their ISOPHOT spectra.

REFERENCES

Blommaert, J., Siebenmorgen, R., Coulais, A., Okumura, K., Ott, S., Sauvage, M., & Starek, J.-L. 2001, *ISO* Handbook, Volume III: CAM—the *ISO* Camera (SAI-99-057/Dc, ver. 1.2; ESA)
Clavel, J., et al. 2000, A&A, 357, 839
Farrah, D., Afonso, J., Efstathiou, A., Rowan-Robinson, M., & Fox, M. 2003, MNRAS, 343, 585
Haas, M., et al. 2003, A&A, 402, 87
Heckman, T. M., O'Dea, C. P., Baum, S. A., & Laurikainen, E. 1994, ApJ, 428, 65
Martel, A. R., Turner, N. J., Sparks, W. B., & Baum, S. A. 2000, ApJS, 130, 267
Meisenheimer, K., et al. 2001, A&A, 372, 719
Ott, S., Pollock, A., & Siebenmorgen, R. 2000, in Leture Notes in Physics 548, *ISO* Surveys of a Dusty Universe, ed. D. Lemke, M. Stickel, & K. Wilke (Berlin: Springer), 283
Prieto, A. M., & Freudling, W. 1993, ApJ, 418, 668
Sanders, D. B., Phinney, E. S., Neugebauer, G., Soifer, B. T., & Mathews, K. 1989, ApJ, 347, 29
Siebenmorgen, Krügel, E., & Spoon, H. W. W. 2003, A&A, in press
Tadhunter, C., & Tsvetanov, Z. 1989, Nature, 341, 422
Urry, C. M., & Padovani, P. 1995, PASP, 107, 803